Bowling Green State University

ScholarWorks@BGSU

11-29-2022

Boost the Lead Conversion Efficiency for the Synthesis of Colloidal 2D PbS Nanosheets

Tharaka MDS Weeraddana
Bowling Green State University

Adam Roach
Bowling Green State University, ajroach@bgsu.edu

Shashini M. Premathilaka
Bowling Green State University

Yiteng Tang
Bowling Green State University

Jordan Fox
Bowling Green State University

Follow this and additional works at: https://scholarworks.bgsu.edu/physics_astronomy_pub

See next page for additional authors

Part of the Astrophysics and Astronomy Commons, and the Physics Commons

How does access to this work benefit you? Let us know!

Repository Citation

Author(s)

Tharaka MDS Weeraddana, Adam Roach, Shashini M. Premathilaka, Yiteng Tang, Jordan Fox, and Liangfeng Sun

Boost the Lead Conversion Efficiency for the Synthesis of Colloidal 2D PbS Nanosheets

Tharaka MDS Weeraddana, Adam Roach, Shashini M. Premathilaka, Yiteng Tang, Jordan Fox, and Liangfeng Sun*

In the synthesis of colloidal PbS nanosheets, the supernatant of the reaction solution is reused to boost the lead conversion efficiency. It doubles the conversion efficiency of the lead precursors to the PbS nanosheets. The nanosheets synthesized by reusing the supernatant have similar morphology, nearly identical thickness, and optical properties as the original ones, confirmed by transmission electron microscopy, X-ray diffraction, and photoluminescence spectroscopy. This method reduces the toxic Pb-containing waste during the synthesis, a step toward the green and scalable synthesis of colloidal 2D PbS nanosheets.

1. Introduction

As one of the emerging colloidal 2D nanomaterials, lead sulfide (PbS) nanosheets[1–17] have demonstrated a thickness tunable bandgap,[5] a highly efficient multiple carrier generation,[18] a narrow emission linewidth,[19] large carrier mobilities,[20] and topological properties.[21] Scalable synthesis of nanomaterials with a high chemical yield is critical for their applications. For instance, people have developed scalable methods to synthesize PbS,[22–24] $CuIn_xGa_{1−x}S_2$,[25] $CsPbBr_3$,[23] and $Cu_3In_5Se_9$ nanocrystals,[23] resulting in more than 10 times the product than that obtained using the traditional method. In the original synthesis of the PbS nanosheets, we need to keep the molar ratio of the feedstock lead (Pb) and sulfur (S) to be 14:1 though the final product has a Pb:S ratio of 1:1.[26] Consequently, about 13/14 of the feedstock lead is not converted into the final product, resulting in toxic Pb-containing waste.

T. MDS Weeraddana, A. Roach, S. M. Premathilaka, Y. Tang, J. Fox, L. Sun
Department of Physics and Astronomy
Bowling Green State University
Bowling Green, OH 43403, USA
E-mail: lsun@bgsu.edu

A. Roach, S. M. Premathilaka, Y. Tang, L. Sun
Center for Photochemical Sciences
Bowling Green State University
Bowling Green, OH 43403, USA

In this work, we report a method that can significantly improve the conversion efficiency of the reactant lead oxide to product lead sulfide nanosheets. It is achieved by reusing the unreacted lead precursor (lead oleate) from the reaction solution. The synthesized nanosheets have nearly identical thickness and optical properties as those obtained in the original synthesis. Minimizing the Pb waste is beneficial for many potential applications of PbS nanosheets, including solar cells,[5,27,28] light-emitting devices,[5,9,19,26,28–30] and transistors.[7,20]

2. Experimental Section

We synthesize the colloidal PbS nanosheets using the method developed earlier (Supporting Information A).[10] Briefly, we mix lead oxide and oleic acid to prepare the lead precursor (lead oleate) and then add chloroalkane as the cosolvent. We mix thioacetamide and trioctylphosphine to prepare the sulfur precursor. When both lead and sulfur precursors are ready, we mix them to react at a set temperature. After the reaction we separate the solid product (nanosheets) using centrifugation. The colorless supernatant is reused for further syntheses.

We load the supernatant in a new flask and heat it to 130 °C under a nitrogen environment (**Figure 1**). We prepare the sulfur precursors in the same way as in the original synthesis and inject them into the flask containing the last supernatant. We stir the mixture for a uniform reaction with a magnetic stir bar at 130 °C for 5 min. Then the reaction solution is cooled down to room temperature to stop the reaction. The nanosheets are separated by centrifuging (3500 RPM, 1576 g), and the supernatant is kept for the next synthesis.

We repeat the procedure 4 times (Figure 1). The solid product separated in each step is washed with toluene in ambient air. We measure the dried product to obtain the mass of the nanosheets. They are 26.1 mg (original), 2.2 mg (first reuse), 9.2 mg (second reuse), and 9.2 mg (third reuse), respectively. Each product is characterized with transmission electron microscopy (TEM), X-ray diffraction (XRD), and photoluminescence (PL) spectroscopy. The samples for PL spectroscopy are prepared by dispersing the nanosheets in tetrachloroethylene. The samples for TEM and XRD are prepared by drop-casting the nanosheets on a TEM grid and a glass substrate, respectively.

The TEM images show the products are PbS nanosheets (**Figure 2**a–d) until the fourth reuse of the supernatant (Figure 2e,f). These nanosheets have rectangular shapes. The
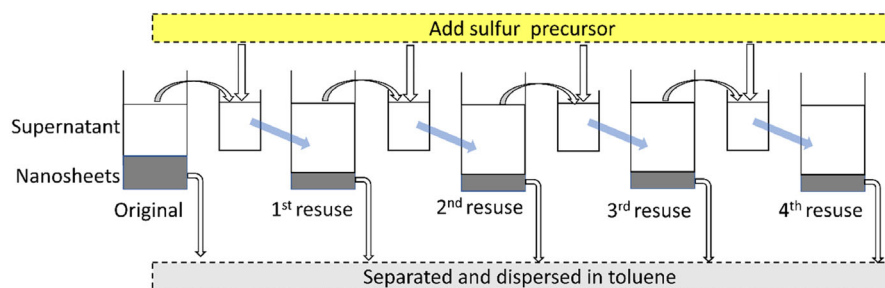
Figure 1. The schematics show the synthesis of nanosheets while reusing the supernatants. The gray shadows indicate the precipitated products.
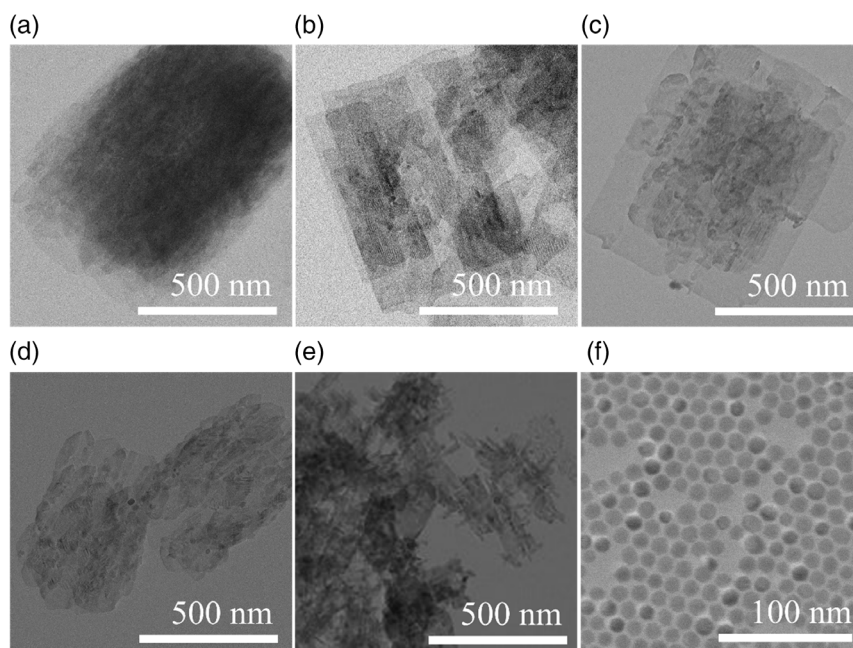

Figure 2. TEM images of the products from a) the original synthesis, b) the first, c) the second, d) the third, and e,f) the fourth reuse of the supernatant.

lateral size decreases after each reuse of the supernatant (Supporting Information B). It is likely due to the decrease of the Pb-to-S ratio in the subsequent synthesis. We estimate the Pb-to-S ratio in each synthesis using the quantities of the reactants and products (Supporting Information C). In the original synthesis, the quantities of Pb and S are 2.267 and 0.160 mmol, respectively. The Pb-to-S ratio is 14:1. After the synthesis, 0.096 mmol of Pb and S converts to PbS nanosheets. The unreacted Pb and S in the supernatant are then 2.171 and 0.064 mmol. We add 0.160 mmol S to the supernatant and reuse it for the following synthesis, where the Pb-to-S ratio turns to 10:1 (**Table 1**). The Pb-to-S ratios are estimated to be 6:1 and 4:1 in the syntheses with the second and third reuses of the supernatant, respectively (Table 1). The reduction in the lateral size follows the decrease in the Pb-to-S ratio in the reaction solution, consistent with the literature.[26]

The product from the fourth reuse of the supernatant is a mixture of narrow nanosheets and quantum dots (Figure 2e,f). In this synthesis, the estimated Pb-to-S ratio is 3:1 (Table 1). Premathilaka and co-workers have shown that the product is

Table 1. The quantities of the lead (Pb) and the sulfur (S) in the reaction solution, the added sulfur, the Pb-to-S molar ratio, and the product PbS nanosheets (NSs) in the original synthesis and the following syntheses with the reuse of the supernatant. The values are based on estimates and calculations detailed in Supporting Information C.

	Pb in solution [mmol]	S in solution [mmol]	S added [mmol]	Pb:S	PbS NSs [mmol]
Original	2.267	0.160	N/A	14:1	0.096
First reuse	2.171	0.064	0.160	10:1	0.008
Second reuse	2.163	0.216	0.160	6:1	0.034
Third reuse	2.129	0.342	0.160	4:1	0.034
Fourth reuse	2.095	0.468	0.160	3:1	N/A

nanosheets when the Pb-to-S ratio is between 2.5:1 and 3.5:1.[26] The product becomes quantum dots when the ratio is 1:1. As to this discrepancy, we speculate that we could overestimate the Pb-to-S ratio in the supernatant. Due to the loss of the

supernatant during the purification process, the actual Pb-to-S ratio in the synthesis is less than what we estimate.

We performed XRD experiments (Supporting Information D) to characterize the products. All the XRD patterns (**Figure 3**) show a peak at ≈30°, matching the diffraction angle (2theta) of the (200) plane of the PbS bulk (galena).[31] The products from the first three syntheses—original, first reuse, and second reuse—show a dominant (200) peak, while other diffraction peaks are negligible (Figure 3a–c). The products from the last two syntheses—third and fourth reuses—show additional peaks at 26.0°, 43.1°, 51.1°, and 53.5° (Figure 3d–e). They are corresponding to the (111), (220), (311), and (222) crystal planes of galena,[31] respectively.

The dominant (200) peak indicates that the basal plane of the nanosheet is the {100} plane.[5] When we prepare the XRD sample by drop-casting the nanosheet solution on a glass substrate, most nanosheets rest on the substrate with their basal planes facing up. Consequently, the (200) peak dominates the XRD pattern. As the lateral size of the nanosheets decreases, they tend to aggregate, making them randomly oriented on the TEM substrate. It results in the multiple XRD peaks (Figure 3d–e). The last

synthesis—fourth reuse—results in dot-like nanocrystals. If they are quantum dots, each dot's orientation is likely random, leading to multiple peaks in the XRD pattern.

The (200) peaks in Figure 3a–c are broad but narrow in Figure 3e. The width of the diffraction peak is inversely proportional to the size of the nanocrystal, as described by the Scherrer equation. Assuming the majority of the nanosheets has their basal plane (200) facing up, we use the dominant (200) peak to estimate the thickness (Supporting Information D). The calculated thickness is ≈3.0 nm for the nanosheets from the first three syntheses (Figure 3a–c), but ≈4.4 nm from the fourth synthesis (third reuse) (Figure 3d). We suspect the random orientation of the nanosheets reduces the width of the diffraction peak, resulting a larger thickness calculated using the Scherrer equation.

The XRD peaks from the last synthesis (Figure 3e) are significant narrower than those from the other syntheses. We calculate the sizes using (111), (200), (220), and (311) peaks, respectively (Supporting Information D). The size ranges from 8 to 11 nm. It is close to the lateral size of the dots revealed by the TEM image (Figure 2f), which likely lead to the narrow multiple XRD peaks shown in Figure 3e.

The nanosheets synthesized by reusing the supernatant exhibit PL spectra close to the original one (**Figure 4**). The wavelength of PL peak from different batches of nanosheets ranges from 1804 to 1860 nm, with an average of 1832 nm and a standard deviation of 19 nm (Supporting Information E). This deviation (19 nm) is much less than the width of the PL peak itself (≈170 nm). Therefore, the average thickness of the nanosheets obtained in each synthesis is nearly the same. The PL peak widths of the nanosheets from different syntheses are also close to each other, indicating their thickness dispersions are close to each other too. The above results show that the thickness and the thickness dispersion remain nearly the same in each synthesis of reusing the supernatant.

We use the PL spectrum from the nanosheets to estimate their average thickness (Figure 4). It is based on the 1D quantum confinement model[5]
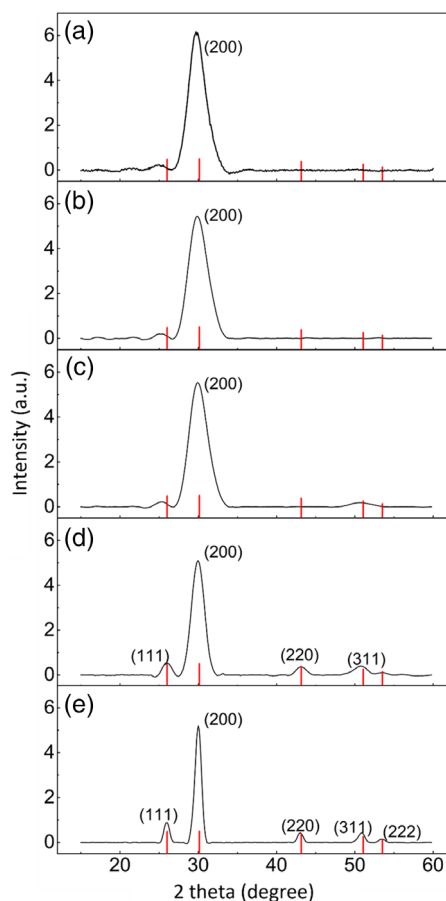

Figure 3. XRD patterns of PbS nanosheets from a) the original, b) the first reuse, c) the second reuse, d) the third reuse, and e) the fourth reuse of the supernatant syntheses. The red lines indicate the diffraction angles (2θ) of the crystal planes of PbS bulk (galena)27 at 26.0° (111), 30.1° (200), 43.1° (220), 51.1° (311), and 53.5° (222), respectively.
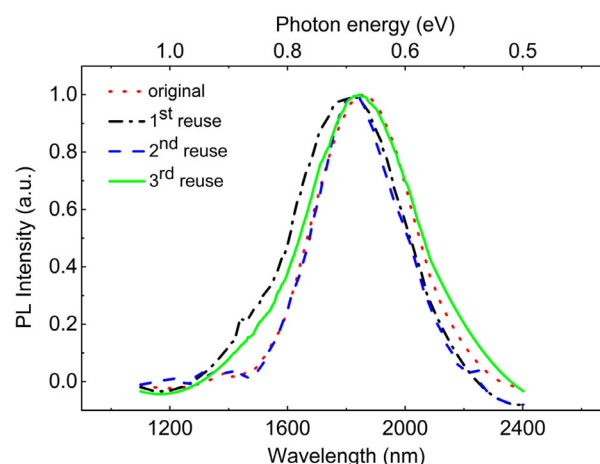

Figure 4. Normalized PL spectra of the nanosheets from the original (dotted line), first reuse (dash-dotted line), second reuse (dashed line), and third reuse (solid line) of the supernatant.

$$E_{gap}(t) = E_{gap}(\infty) + \frac{1}{0.99t + 1.18} \qquad (1)$$

The energy gap of bulk PbS—$E_{gap}(\infty)$—is 0.41 eV at room temperature. The energy gap of the nanosheets—$E_{gap}(t)$—depends on its thickness t. The model shows the energy gap of the nanosheet increases as its thickness decreases. As the energy of the photon emitted by the nanosheet is close to the energy gap of the nanosheet, we use the central photon energy (E_{photon}) of the PL to estimate the thickness.

The derived thicknesses of the nanosheets from the first three syntheses (original, first reuse, and second reuse) are 2.7, 2.4, and 2.6 nm, respectively (**Table 2**). They are slightly thinner ($\approx$0.5 nm) than those obtained from the XRD peaks: 3.2, 2.9, and 3.0 nm, respectively. It indicates there is a systematic error in either the confinement model or the Scherrer model. The derived thickness of the nanosheets from the fourth synthesis (third reuse) is 2.7 nm. It is close to the thickness of other nanosheets derived from the PL spectra but much less than that obtained from XRD (4.4 nm). The latter, however, is not reliable because of the random orientation of the nanosheets on the XRD peak.

The conversion efficiencies of the reactants in the reusing syntheses are less than the original ones. We define conversion efficiency as the molar ratio of the element in the product to the same one in the reactant. The variation of the conversion efficiencies is repeatable, confirmed in our experiments (Supporting Information F). In the original synthesis, the average conversion efficiency of Pb and S is 4.3% and 61.3%, respectively. In the first synthesis of the reused supernatant, they all drop significantly (**Figure 5**). Then they recover some in the following two syntheses. The concentration of the lead precursor (lead oleate) remains nearly the same in all the syntheses, but the concentration of the sulfur precursor increases in each succeeding synthesis (Table 1). It indicates that the lead conversion efficiency depends on the Pb-to-S ratio (or the sulfur concentration) in the reaction solution.

To reveal if the same lead conversion efficiency as in the original synthesis can be achieved in the synthesis with the reuse of the supernatant, we design a new experiment by adding 0.09 mmol sulfur to the supernatant after the original synthesis, making the Pb:S ratio 14:1 (the same as that in the original synthesis). The quantity of nanosheets we get is 8.8 mg, much less than what we got in the original synthesis ($\approx$26.6 mg). We suspect that the lead and sulfur precursors in the supernatant have different chemical reactivity from those in the original reaction solution. We notice that the reaction solution takes a long time to change its color in contrast to the original synthesis.

Table 2. The central photon energy (E_{photon}) and the standard deviation (σ_{photon}) of the PL peak from the nanosheets of each synthesis. The calculated thickness (t) and the standard deviation (σ_t) of the nanosheets.

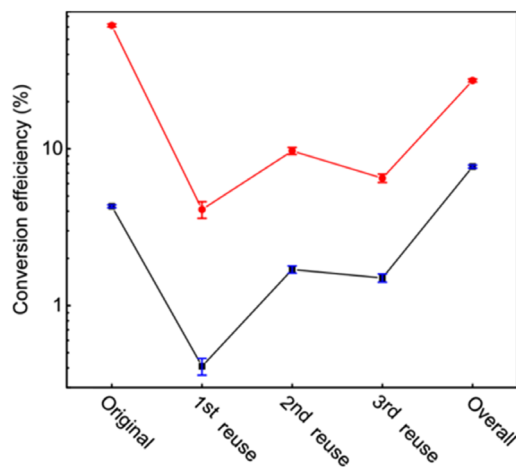| Synthesis	E_{photon} [eV]	σ_{photon} [eV]	t [nm]	σ_t [nm]
Original	0.67	0.057	2.7	0.8
First reuse	0.69	0.063	2.4	0.8
Second reuse	0.68	0.056	2.6	0.7
Third reuse	0.67	0.062	2.7	0.9

Figure 5. The conversion efficiency of Pb (solid squares) and S (solid circles) in each synthesis. The lines are to guide the eyes. The error bars indicate the batch-to-batch variation of the sample.

It indicates a lower reactivity, which leads to lower conversion efficiencies.

The change of the chloroalkane—1,1,2-trichloroethane (TCA) concentration—and the accumulation of the by-products in the reaction solution probably affect the reaction dynamics too. As TCA is volatile, its amount reduces after each synthesis shown in Figure 1. On the other hand, the sulfur amount increases, making a lower TCA:S ratio in each sequential synthesis. It may contribute to the decrease in the lateral size of the nanosheet, as we demonstrated earlier.[26] The by-products include amines (from thioacetamide) which are one type of surface ligands for colloidal nanocrystals. They may affect the growth dynamics (e.g., the lateral growth) of the nanosheets.

The supernatant reuse increases the overall Pb conversion efficiency. The total quantity of the PbS nanosheets synthesized is 47.6 mg, nearly twice as much as that in the original synthesis (26.6 mg). In the original synthesis, only 4.3% of the Pb converts to PbS nanosheets (Figure 5). Three reuses of the supernatant increase the conversion efficiency to 7.7%. The conversion efficiency of sulfur is higher than lead in each synthesis and variates in the same pattern as lead (Figure 5). The overall sulfur conversion efficiency, however, drops down to 27.3%.

This method may be applicable for other syntheses where the ratio of the reactants is very different from the stoichiometric ratio of the product. For instance, in the synthesis of PbS nanosheets developed by Bielewica and co-workers,[7] the ratio of lead-to-sulfur is kept at a high value (Pb:S = 120:1). In that synthesis, less than 1% of the reactant lead converts to PbS nanosheets. If our method is applied in that synthesis, the conversion efficiency of the reactant lead could be significantly improved.

3. Conclusions

We develop a method to improve the lead conversion efficiency in the synthesis of colloidal PbS nanosheets. The reuse of the supernatant in the follow-up syntheses doubles the overall lead conversion efficiency. The synthesized nanosheets using

the supernatant have nearly identical thickness and optical properties to the original ones. This method reduces the toxic lead-containing waste in the synthesis, a step toward the green synthesis of PbS nanosheets. It may also help the scalable synthesis of the colloidal PbS nanosheets, an emerging nanomaterial for infrared optoelectronic devices.

Supporting Information

Supporting Information is available from the Wiley Online Library or from the author.

Conflict of Interest

The authors declare no conflict of interest.

Data Availability Statement

The data that support the findings of this study are available in the supplementary material of this article.

[1] S. Acharya, D. D. Sarma, Y. Golan, S. Sengupta, K. Ariga, *J. Am. Chem. Soc.* **2009**, *131*, 11282.
[2] C. Schliehe, B. H. Juarez, M. Pelletier, S. Jander, D. Greshnykh, M. Nagel, A. Meyer, S. Foerster, A. Kornowski, C. Klinke, H. Weller, *Science* **2010**, *329*, 550.
[3] Z. Wang, C. Schliehe, T. Wang, Y. Nagaoka, Y. C. Cao, W. A. Bassett, H. Wu, H. Fan, H. Weller, *J. Am. Chem. Soc.* **2011**, *133*, 14484.
[4] S. Acharya, B. Das, U. Thupakula, K. Ariga, D. D. Sarma, J. Israelachvili, Y. Golan, *Nano Lett.* **2013**, *13*, 409.
[5] G. B. Bhandari, K. Subedi, Y. He, Z. Jiang, M. Leopold, N. Reilly, H. P. Lu, A. T. Zayak, L. Sun, *Chem. Mater.* **2014**, *26*, 5433.
[6] P. J. Morrison, R. A. Loomis, W. E. Buhro, *Chem. Mater.* **2014**, *26*, 5012.
[7] T. Bielewicz, S. Dogan, C. Klinke, *Small* **2015**, *11*, 826.
[8] T. Bielewicz, M. M. Ramin Moayed, V. Lebedeva, C. Strelow, A. Rieckmann, C. Klinke, *Chem. Mater.* **2015**, *27*, 8248.
[9] S. Khan, Z. Jiang, S. M. Premathilka, A. Antu, J. Hu, A. A. Voevodin, P. J. Roland, R. J. Ellingson, L. Sun, *Chem. Mater.* **2016**, *28*, 5342.
[10] S. M. Premathilaka, Z. Jiang, A. Antu, J. Leffler, J. Hu, A. Roy, L. Sun, *Phys. Status Solidi RRL* **2016**, *10*, 838.
[11] T. Bielewicz, E. Klein, C. Klinke, *Nanotechnology* **2016**, *27*, 355602.
[12] H. Zhang, B. H. Savitzky, J. Yang, J. T. Newman, K. A. Perez, B. Hyun, L. F. Kourkoutis, T. Hanrath, F. W. Wise, *Chem. Mater.* **2016**, *28*, 127.
[13] S. M. Premathilaka, Z. Jiang, A. Antu, J. Leffler, J. Hu, A. Roy, L. Sun, *MRS Adv.* **2017**, *2*, 3703.
[14] S. Khan, Z. Jiang, S. M. Premathilka, J. Hu, A. Voevodin, P. J. Roland, R. J. Ellingson, L. Sun, *MRS Adv.* **2017**, *2*, 3685.
[15] A. H. Khan, R. Brescia, A. Polovitsyn, I. Angeloni, B. Martín-García, I. Moreels, *Chem. Mater.* **2017**, *29*, 2883.
[16] M. Shkir, S. AlFaify, V. Ganesh, I. S. Yahia, *Solid State Sci.* **2017**, *70*, 81.
[17] Q. A. Akkerman, B. Martín-García, J. Buha, G. Almeida, S. Toso, S. Marras, F. Bonaccorso, U. Petralanda, I. Infante, L. Manna, *Chem. Mater.* **2019**, *31*, 8145.
[18] M. Aerts, T. Bielewicz, C. Klinke, F. C. Grozema, A. J. Houtepen, J. M. Schins, L. D. A. Siebbeles, *Nat. Commun.* **2014**, *5*, 3789.
[19] Z. Jiang, G. B. Bhandari, S. M. Premathilaka, S. Khan, D. M. Dimick, C. Stombaugh, A. Mandell, Y. He, H. Peter Lu, L. Sun, *Phys. Chem. Chem. Phys.* **2015**, *17*, 23303.
[20] S. Dogan, T. Bielewicz, Y. Cai, C. Klinke, *Appl. Phys. Lett.* **2012**, *101*, 073102.
[21] W. Wan, Y. Yao, L. Sun, C. Liu, F. Zhang, *Adv. Mater.* **2017**, *29*, 1604788.
[22] J. Zhang, J. Gao, E. M. Miller, J. M. Luther, M. C. Beard, *ACS Nano* **2014**, *8*, 614.
[23] M. Yarema, O. Yarema, W. M. M. Lin, S. Volk, N. Yazdani, D. Bozyigit, V. Wood, *Chem. Mater.* **2017**, *29*, 796.
[24] A. Preske, J. Liu, O. V. Prezhdo, T. D. Krauss, *ChemPhysChem* **2016**, *17*, 681.
[25] E. Dilena, Y. Xie, R. Brescia, M. Prato, L. Maserati, R. Krahne, A. Paolella, G. Bertoni, M. Povia, I. Moreels, L. Manna, *Chem. Mater.* **2013**, *25*, 3180.
[26] S. M. Premathilaka, Y. Tang, Z. Jiang, T. M. D. S. Weeraddana, A. Debnath Antu, S. Bischoff, L. Sun, *ChemNanoMat* **2020**, *6*, 816.
[27] S. Dogan, T. Bielewicz, V. Lebedeva, C. Klinke, *Nanoscale* **2015**, *7*, 4875.
[28] T. M. D. S. Weeraddana, S. M. Premathilaka, Y. Tang, A. D. Antu, A. Roach, J. Yang, L. Sun, *J. Phys. Chem. Lett.* **2022**, *13*, 7756.
[29] A. D. Antu, Z. Jiang, S. M. Premathilka, Y. Tang, J. Hu, A. Roy, L. Sun, *Chem. Mater.* **2018**, *30*, 3697.
[30] Z. Jiang, Y. Tang, A. D. Antu, S. M. Premathilaka, M. L. Cayer, C. A. Heckman, P. Moroz, M. Zamkov, L. Sun, *J. Phys. Chem. Lett.* **2022**, *13*, 8987.
[31] Y. Noda, K. Masumoto, S. Ohba, Y. Saito, K. Toriumi, Y. Iwata, I. Shibuya, *Acta Cryst. C* **1987**, *43*, 1443.